SURFACE FEATURES AND BRINE CONVECTION IN THE MARTIAN NEAR-SURFACE. B. J. Travis[1] and W. C. Feldman[2], [1]Computational Earth Science Group, EES-16/MS-J535, Los Alamos National Laboratory, Los Alamos, NM 87545, bjtravis@lanl.gov, [2]Planetary Science Institute, Tucson, AZ, feldman@psi.edu.

Introduction: Hydrothermal circulation of brines in the subsurface of Mars is a possible mechanism that can deposit ice, and brine, close to, or even at, the surface of Mars. Freezing and thawing patterns associated with brine convection may be related to some observed surface features such as polygonal ground. In this study, numerical simulations of brine convection in cold soil with resulting heaving/slumping of soil under Martian conditions produce polygonal patterns similar to observed surface features.

Model: A previous simulation study of aquifer dynamics in the Martian subsurface considered only pure water systems [1]. It found that hydrothermal convection develops for a range of geothermal gradients, for reasonable soil properties, but that pure-water-convecting systems cannot exist very close to the cold Martian surface. Subsequent experimental and numerical studies [2, 3] considered salty aquifer dynamics in response to a geothermal gradient under a freezing surface. Some salts, such as $CaCl_2$ and some ferric chlorides, can depress freezing points by 50 to 70 ^oC. Salt not only depresses the freezing point but can add an unsteady characteristic to hydrothermal convection [2]. Simulations reported here make use of the MAGHNUM code. MAGHNUM solves the time-dependent governing equations for water and vapor flow, and heat and salt transport in cold, porous, permeable media in 1-D, 2-D or 3-D geometries. It allows transformations between liquid, vapor and ice phases, depending on local thermodynamics. Thermal conductivity and specific heat are volume fraction-weighted averages of the thermal conductivities and specific heats of soil, water, ice and air, each of which is temperature dependent. Chemical, as well as thermal, buoyancy is an important factor in driving flow. Fluid density is a function of temperature and salt content. Fluid viscosity depends on temperature and salt content, and is based on experimental data [2]. At the eutectic, fluid viscosity is more than an order of magnitude greater than for pure water above freezing. Salt precipitation and dissolution are computed by partitioning salt between fluid and solid phases according to the salt's binary phase graph.

Surface Deformation: Freezing of water and melting of ice result in volume changes, which in turn, leads to either heaving of soil (upon freezing) or slumping (upon melting of ice). We have estimated the surface deformation, that is, spatial distribution of elevation change, due to the spatial pattern of subsurface ice formation in our model simulations, by integrating volume change over depth, that is,

$$\Delta z(x) = \int i(x,z)\, \varepsilon(x,z)\, (\rho w - \rho i)/\rho w \; dz$$

where Δz is the local surface elevation (compared to an unfrozen soil), $i(x,z)$ is the local ice fraction, $\varepsilon(x,z)$ is local porosity, ρi and ρw are ice and water densities. Results are summarized below for a couple of simulations taken from a set of 2-D and 3-D simulations. Model domains are 200 m x 200 m for 2-D (x-z) simulations and 200x200x200 m for 3-D simulations; grid node spacing is 1 or 2 m. Simulations consider a range of permeabilities (10-1000 darcies), geothermal heat fluxes (20-60 mW/m^2) and initial salt contents (5-29%wt); surface temperature is -52 ^oC.

Figure 1 is a plot of surface elevation change (relative to the average elevation change) vs horizontal location for one of the 2-D cases, and Figure 2 is a plot of surface elevation vs horizontal location for one of the

3-D simulations. Generally, the average uplift is in the 0.5 to 2 m range, with variations in topography superimposed. A general result is that margins and troughs are typically deeper than mounds are high. Mounds overlie ice lenses in the upwelling regions, while troughs overlie downwellings that are ice-poor. The elevation difference between mound height and the surrounding trench depression is roughly 0.35 m to 1.50 m. The size of polygons at the surface is roughly 20 m in the 2-D case. The 3-D case shows more variability in polygon sizes, with some up to 50-60 m, as well as smaller ones. Figures 1 and 2 correspond to high initial salt concentration. Other simulations (not shown) starting from an initially low pore water salt concentration case result in a very different surface deformation pattern, yielding a field of surface pits that are a few meters in diameter, with depths that vary from fractions of a meter, to several meters.

Discussion: Polygonal ground on Mars is widespread [4, 5, 6] and is seen generally at high northern latitudes [7], in Athabasca Valles, Elysium basin, Marte Vallis, western Amazonis Planitia, as well as the Cerberus Fossae region [8, 9]. At many sites, polygon diameters range roughly from 10 to 20 meters, in agreement with sizes that have been shown to result from thermal contraction in ice-rich permafrost [10]. Polygons are also frequently observed near stone circles, another feature of periglacial activity [9]. Sorted patterned ground on Earth results from freeze-thaw cycling and cryoturbation. Some polygons have positive, some have negative relief margins, more often domed, with diameters of 10-20 m, although some are as large as 40 m. The polygonal patterns from our numerical simulations cover the range of observed polygon sizes.

References: [1] Travis B. J. et al (2003) *JGR, 108*, 8040-8052. [2] McGraw et al (2006) *LPS XXXVII*, 2224. [3] Travis B. J. and Feldman W. C. (2009) *LPS XL*, 1315. [4] Mangold N. S. et al (2004) *JGR 109,* E08001. [5] Mangold N. S. (2005) *Icarus, 174,* 336-359. [6] Levy J. et al (2009) *JGR 114*, E01007. [7] Mellon M. T. et al (2008) *JGR 113,* E00A23. [8] Page D. P. and Murray J. B. (2006) *Icarus 183,* 46-54. [9] Balme M. R. and Gallagher C. (2009) *EPSL* doi:10.1016/j.epsl.2009.05.031. [10] Mellon M. T. (1997) *JGR, 102*, 25617-25628.

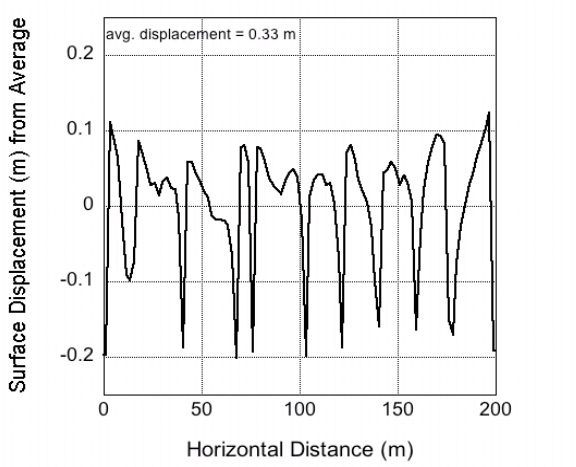

Figure 1 Surface displacement vs horizontal position for a 2-D simulation.

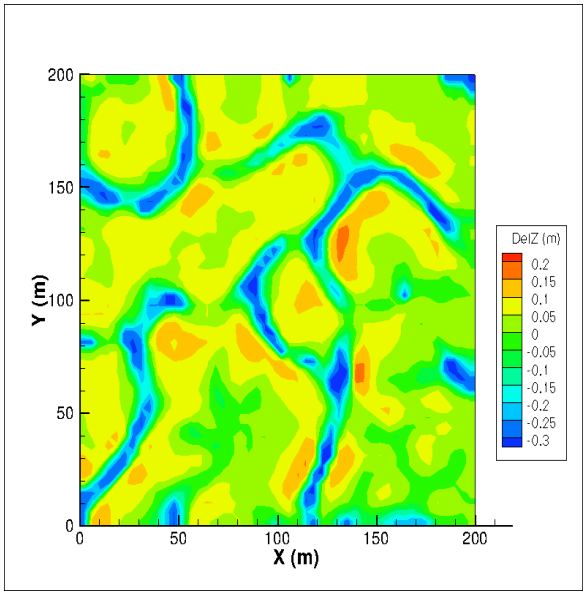

Figure 2 Two-dimensional distribution of surface displacement for a typical 3-D simulation.